



Exploring orientationally aligned anisotropic large spin molecules with unusual long-distance intermolecular ferromagnetic interactions

Journal:	<i>Journal of Materials Chemistry C</i>
Manuscript ID	TC-ART-02-2019-000740.R1
Article Type:	Paper
Date Submitted by the Author:	15-Mar-2019
Complete List of Authors:	Minato, Takuo; The University of Tokyo, Department of Applied Chemistry, School of Engineering, Ohata, Yusuke; The University of Tokyo, Department of Applied Chemistry, School of Engineering, Ishii, Kazuyuki; The University of Tokyo, Institute of Industrial Science Yamaguchi, Kazuya; The University of Tokyo, Department of Applied Chemistry Mizuno, Noritaka; The University of Tokyo, Department of Applied Chemistry Suzuki, Kosuke; The University of Tokyo, Department of Applied Chemistry, School of Engineering,

Exploring orientationally aligned anisotropic large spin molecules with unusual long-distance intermolecular ferromagnetic interactions†

Takuo Minato,^a Yusuke Ohata,^a Kazuyuki Ishii,^b Kazuya Yamaguchi,^a Noritaka Mizuno^a
and Kosuke Suzuki *^{a,c}

^a Department of Applied Chemistry, School of Engineering, The University of Tokyo, 7-3-1 Hongo, Bunkyo-ku, Tokyo 113-8656, Japan. E-mail: ksuzuki@appchem.t.u-tokyo.ac.jp

^b Institute of Industrial Science, The University of Tokyo, 4-6-1 Komaba, Meguro-ku, Tokyo 153-8505, Japan

^c Precursory Research for Embryonic Science and Technology (PRESTO), Japan Science and Technology Agency (JST), 4-1-8 Honcho, Kawaguchi, Saitama 332-0012, Japan

† Electronic supplementary information (ESI) available: Tables S1–S6, Fig. S1–S13.

Abstract

Anisotropic magnetic clusters are interesting materials because magnetic anisotropy and spin state are important factors in their magnetic properties. Although long-distance magnetic interactions have been observed in several assemblies of anisotropic magnetic molecules, these interactions are small and observed at extremely low temperature (typically below 2 K). In this work, to assemble orientationally aligned anisotropic large spin metal oxo clusters, we managed to synthesize a $\{V^{3+}Mn^{3+}_4\}$ cluster with a large-spin ($S_T = 9$) ground state by utilizing an anisotropic lacunary polyoxometalate template. In the orientationally aligned clusters, unusual long-distance intermolecular ferromagnetic interactions were induced below 35 K by a small magnetic field (> 0.01 T).

Introduction

Assemblies of anisotropic molecules, clusters, and nanoparticles are of growing interest because orientationally aligned anisotropic particles exhibit unique optical, magnetic, and electrochemical properties, leading to the functional materials such as liquid-crystal display, magnetic storage materials, and band gap materials.¹⁻³ Anisotropic magnetic clusters are intrinsically interesting because the magnetic anisotropy and spin state of clusters play important roles to control the magnetic properties.⁴ In addition to the design of each molecule, orientation of magnetic clusters in the crystals is also important.^{5,6} Although the interactions were significantly small and observed only at low temperature (typically, below 2 K), several large spin molecules exhibiting magnetic ordering via magnetic dipole interactions have been reported to date: for example, $\text{Hpy}[\text{Fe}_{17}\text{O}_{16}(\text{OH})_{12}(\text{py})_{12}\text{Br}_4]\text{Br}_4$ and $\text{Mn}_6\text{O}_4\text{Br}_4\text{L}_6$.⁵⁻¹³ In addition, there have been several studies on the effect of magnetic anisotropy on dipole interaction in bulk magnetic compounds.^{14,15} What would happen if magnetic clusters possessing both large spin and large magnetic anisotropy were orientationally aligned?

To approach the question, we set about seeing if we could utilize polyoxometalate (POM)-based fragments.¹⁶⁻²¹ Lacunary POMs (ex. $[\text{A}-\alpha\text{-SiW}_9\text{O}_{34}]^{10-}$) act as rigid anisotropic multidentate ligands for constructing anisotropic multinuclear metal oxo cluster. Recently, we have developed the sequential synthesis method for constructing heteromultinuclear metal oxo clusters within lacunary POMs.²²⁻²⁵ By tailoring the combination of metal cations, intramolecular superexchange interactions and single-molecule magnet (SMM) properties can be controlled, potentially allowing the design of large spin clusters. In addition, the axial ligands of metal cations are aligned to the same direction, and the large uniaxial magnetic anisotropy could be achieved. In this study, we have synthesized an anisotropic heteropentanuclear metal oxo cluster $\{\text{V}^{3+}\text{Mn}^{3+}_4\}$ within anisotropic trivacant lacunary POMs ($\text{TBA}_7[(\text{A}-\alpha\text{-SiW}_9\text{O}_{34})_2\text{VMn}_4(\text{OH})_2]$ (**II**), TBA = tetra-*n*-butylammonium; Fig. 1 and 2). The intramolecular ferromagnetic superexchange interactions between the suitably

arranged one V^{3+} ($S = 1$) and four Mn^{3+} ($S = 2$) cations successfully engendered a large spin ($S_T = 1 + 2 \times 4 = 9$). Furthermore, we could control the arrangement of **II** in the crystalline state to prepare orientationally aligned and non-aligned POMs with two types of orientations, and discovered that the orientationally aligned anisotropic large-spin molecules (**II-a**) exhibited unusual long distance intermolecular ferromagnetic interactions below 35 K under a small magnetic field.

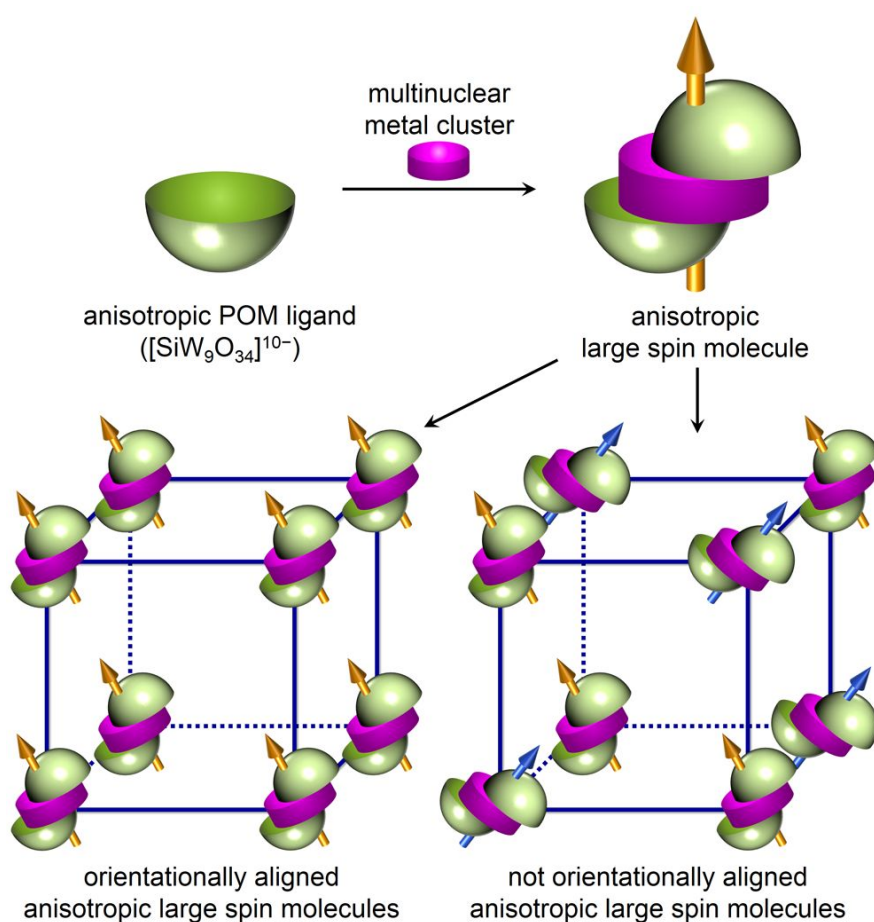


Fig. 1 Schematics of preparation of orientationally aligned/not aligned anisotropic large spin molecules in the crystal by using an anisotropic lacunary POM ligand. The green and purple solid figures represent POM frameworks and multinuclear metal oxo clusters, respectively. Arrows represent the anisotropies of metal oxo clusters.

Results and discussion

Synthesis of a mononuclear V³⁺-containing POM (**I**)

Initially, a V³⁺-containing POM (**I**) was synthesized by reacting TBA₄H₆[A- α -SiW₉O₃₄] \cdot 2H₂O (**SiW9**)²⁶ with 0.5 equivalents of V(acac)₃ (acac = acetylacetonate) in a mixture of acetone and water (17:3, v/v) under Ar.²⁷ X-ray crystallographic analysis revealed that the product is a vanadium-containing S-shaped dimer possessing vacant sites (Table 1, Fig. S1a, ESI[†]). The bond valence sum (BVS) values for W (5.74–6.18), Si (3.86), and V (2.95) indicate that their respective valences are +6, +4, and +3 (Table S1, ESI[†]). The X-ray photoelectron spectroscopy (XPS) spectrum in the V2p region presented peaks for V2p_{3/2} (515.1 eV) and V2p_{1/2} (ca. 523 eV) (Fig. 3a). The binding energy of V2p_{3/2} (515.1 eV) was close to that of V₂O₃ (515.29 \pm 0.2 eV), confirming that V species exists as V³⁺.²⁸ The direct current (dc) magnetic susceptibility data of polycrystalline samples of **I** supported the valence of V³⁺ (Fig. S2a, ESI[†]).²⁹ Based on these data, elemental analysis, and TG analysis, the formula of **I** is TBA₇H₁₀[(A- α -SiW₉O₃₄)₂V] \cdot 2H₂O \cdot C₂H₄Cl₂. It is noteworthy that **I** is the first reported example of a V³⁺-containing heteropolyoxometalate.^{30–32}

Synthesis of V³⁺–Mn³⁺-containing POMs (**II-a**, **II-b**)

Next, a V³⁺–Mn³⁺ heteropentanuclear cluster (**II**) was synthesized by reacting **I** with four equivalents of Mn(acac)₃. Upon addition of diethyl ether to the reaction solution of **II** in 1,2-dichloroethane, dark-purple single crystals (**II-a**) were successfully obtained. The CSI mass spectrum of a 1,2-dichloroethane solution of the crystals gave sets of signals at *m/z* 3471 and 6698 assignable to [TBA₉H₂Si₂W₁₈O₇₀VMn₄]²⁺ and [TBA₈H₂Si₂W₁₈O₇₀VMn₄]⁺, respectively, indicating that four manganese cations were introduced into the vacant sites of **I** (Fig. S3b). X-ray crystallographic analysis revealed that the anion structure of **II** consists of a {VMn₄} cluster and two sandwiching [A- α -SiW₉O₃₄]¹⁰⁻ units (Table 1, Fig. 2a, 2b, and S1b, ESI[†]). The BVS values for W (5.98–6.11), Si (3.98, 3.99), V (2.93), and Mn (2.97–3.00) indicate that their respective valences

are +6, +4, +3, and +3 (Table S2, ESI†). The XPS spectrum in the V2p region showed no significant difference to that of **I**, i.e., the binding energy for V2p_{3/2} (515.2 eV) was close to those of V₂O₃ (515.29 ± 0.2 eV) and **I** (515.1 eV), supporting the obtained valence of V³⁺ in **II** (Fig. 3b).

Thus, the results discussed above, as well as the elemental analysis and thermogravimetric (TG) analysis data, indicate that the formula of the product is TBA₇[(A- α -SiW₉O₃₄)₂VMn₄(OH)₂]·H₂O (**II-a**) and that the crystals contain no paramagnetic impurities. The Jahn-Teller axes of a {VMn₄} cluster were aligned by using anisotropic SiW₉ ligands, resulted in the construction of a designed anisotropic molecule (Table S4, ESI†). It is noteworthy that a V³⁺-Mn³⁺ heteromultinuclear metal oxo cluster have no precedent before **II**.

Crucially, the molecular orientations in the crystals could be controlled by selecting crystallization solvents. When diethyl ether was added to the synthesis solution of **II** in 1,2-dichloroethane, single crystals with orientationally aligned clusters were obtained (**II-a**; Fig. 1, 2c, and 4a-c). In contrast, by recrystallization from a mixture of nitromethane and diethyl ether, single crystals of clusters with two types of orientations were obtained (**II-b**; Fig. 1, 2d, and 4d-f). X-ray crystallographic analysis and CSI mass spectrum revealed that the anion structure in **II-b** is essentially isostructural with that in **II-a** (Table 1, Fig. S1c and S3c, ESI†), i.e., the bond lengths, angles, and BVS values of the {VMn₄} cluster in **II-b** are the same as those in **II-a** (Tables S2–S5, ESI†). Based on these data, elemental analysis, and TG analysis, the formula of **II-b** is TBA₇[(SiW₉O₃₄)₂VMn₄(OH)₂]·10H₂O·CH₃NO₂. Thus, orientationally aligned (**II-a**) and not aligned (**II-b**) anisotropic molecules in the crystalline state were successfully synthesized; i.e., **II-a** exhibits molecules aligned in one direction, whereas **II-b** exhibits molecules with two different orientations possessing mirror image relation, which were packed in alternating layers. The distance between the central V³⁺ in the nearest neighboring anions is ca. 14 Å for both **II-a** and **II-b**, and each anion is separated by TBA cations and solvents of crystallization (Fig. 4c).

Table 1. Crystallographic data of **I**, **II-a**, and **II-b**

	I	II-a	II-b
molecular formula	C ₁₂₄ Cl ₁₂ N ₇ O ₇₀ Si ₂ VW ₁₈	C ₁₂₀ Cl ₈ Mn ₄ N ₇ O ₇₀ Si ₂ VW ₁₈	C ₁₁₆ Mn ₄ N ₁₁ O ₇₈ Si ₂ VW ₁₈
Fw (g mol ⁻¹)	6549.13	6579.05	6431.45
crystal system	triclinic	triclinic	monoclinic
space group	<i>P</i> -1 (No. 2)	<i>P</i> -1 (No. 2)	<i>P</i> 2 ₁ / <i>c</i> (No. 14)
<i>a</i> (Å)	14.6894(4)	14.32330(10)	28.5552(2)
<i>b</i> (Å)	18.7501(3)	20.1223(2)	22.3557(2)
<i>c</i> (Å)	19.1270(5)	34.2013(4)	29.6380(2)
<i>α</i> (deg)	107.0720(10)	102.5640(10)	90
<i>β</i> (deg)	91.9510(10)	96.6350(10)	105.0709(2)
<i>γ</i> (deg)	97.900(2)	93.4300(10)	90
volume (Å ³)	4972.8(2)	9520.16(17)	18269.3(2)
<i>Z</i>	1	2	4
temp (K)	123(2)	123(2)	123(2)
ρ_{calcd} (g cm ⁻³)	2.187	2.295	2.338
GOF	1.111	1.111	1.155
R_1^a [$I > 2\sigma(I)$]	0.0954	0.0576	0.0487
wR_2^a	0.2986	0.1881	0.1510

$$^a R_1 = \sum ||F_o| - |F_c|| / \sum |F_o|, wR_2 = \{ \sum [w(F_o^2 - F_c^2)] / \sum [w(F_o^2)] \}^{1/2}.$$

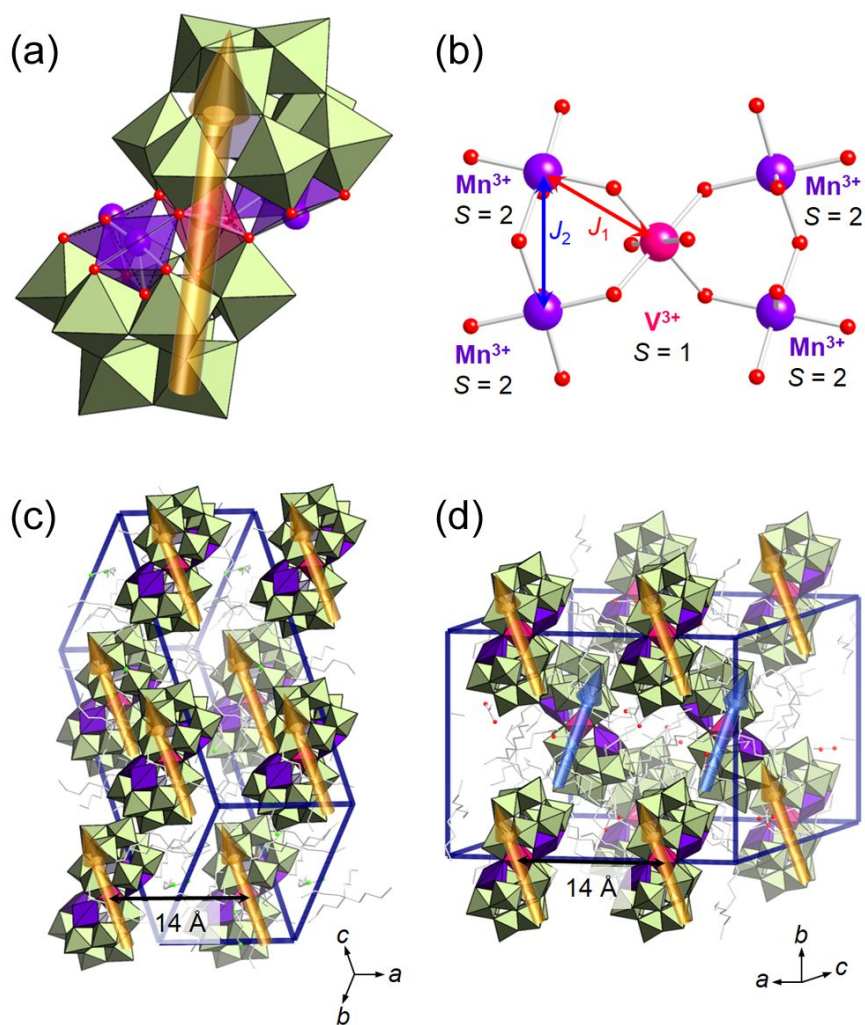


Fig. 2 (a) Polyhedral representation of **II**, (b) ball-and-stick representation of a $\{VMn_4\}$ cluster, and crystal packings of (c) **II-a** and (d) **II-b**. Green, gray, pink, and purple polyhedra represent $[WO_6]^{6-}$, $[SiO_4]^{4-}$, $[VO_6]^{9-}$, and $[MnO_5]^{7-}$, respectively. Red and light-green spheres represent O and Cl atoms, respectively. Gray sticks in (c) and (d) represent TBA cations and solvents of crystallization.

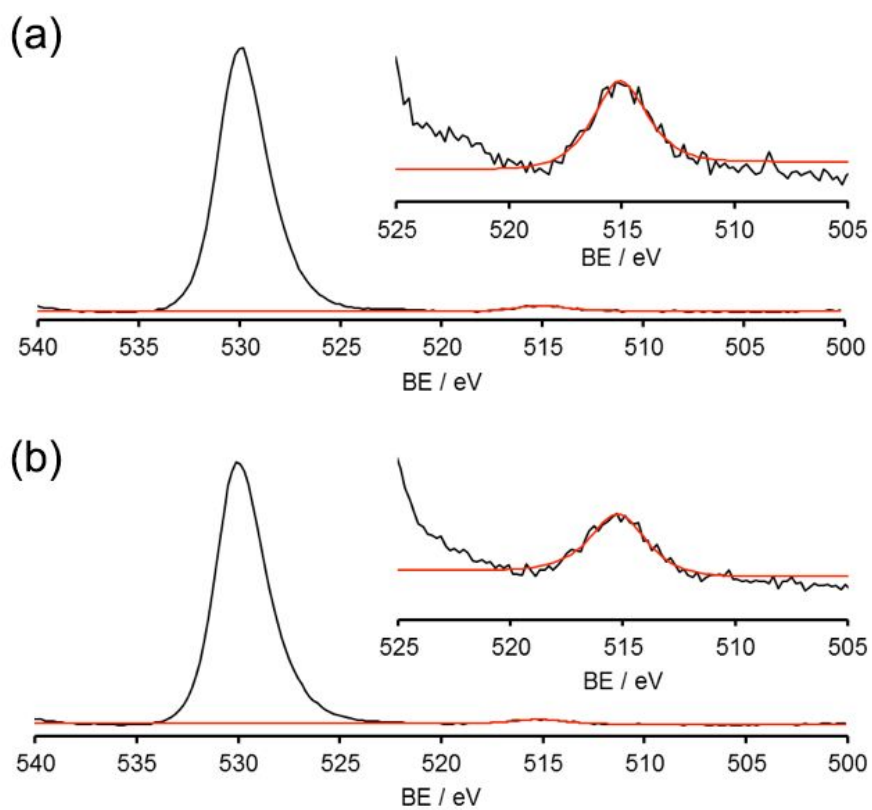


Fig. 3 XPS spectra of (a) **I** and (b) **II-a**. The red lines represent the best fitting curves.

Magnetic properties of **II-a** and **II-b**

To investigate the magnetic properties of **II-a** and **II-b**, dc magnetic susceptibility measurements were performed. These compounds exhibited similar dc magnetic susceptibility data under a very small magnetic field (Fig. 5a and S4, ESI†).³³ The χT values continuously increased with decreasing temperature and reach $46.0 \text{ cm}^3 \text{ K mol}^{-1}$ (**II-a**, 0.005 T) and $39.8 \text{ cm}^3 \text{ K mol}^{-1}$ (**II-b**, 0.02 T) at 1.9 K, indicating intramolecular ferromagnetic interactions and a spin ground state of 9 (expected χT value: $45 \text{ cm}^3 \text{ K mol}^{-1}$). The temperature dependences of the inverse magnetic susceptibilities (χ^{-1}) for **II-a** and **II-b** obeyed the Curie-Weiss law above 100 K affording the positive Weiss constants, supporting the dominant ferromagnetic exchange interactions (Fig. S5, ESI†). The M vs. HT^{-1} data supported the spin ground state of $S_T = 9$ (Fig. 5b).^{34,35} The alternating current magnetic susceptibilities for **II-a** and **II-b** showed the slow relaxation of magnetization characteristic for SMMs under a zero dc field, supporting the large uniaxial magnetic anisotropy (Fig. S6 and S7, ESI†).

By increasing the magnetic fields to 0.1 T, the χT values for **II-b** slightly decreased at low temperature (Fig. S4, ESI†). In contrast, very interestingly, the χT values for **II-a** were strongly dependent on the magnetic field. The maximum χT value for **II-a** increased with increasing the magnetic field (from 0.005 to 0.1 T) and reached $101.79 \text{ cm}^3 \text{ K mol}^{-1}$ at 2.9 K under 0.1 T (Fig. 5a), which was significantly larger than the expected maximum value for the cluster with $S_T = 9$ ($45 \text{ cm}^3 \text{ K mol}^{-1}$). These results indicated that the intermolecular ferromagnetic interactions were induced even by the significantly small magnetic field (0.01–0.1 T) in the case of **II-a**. The $\Delta\chi T$ curve, which was obtained by subtracting the χT curve of **II-b** from that of **II-a**, clearly revealed the abrupt increase of $\Delta\chi T$ at ca. 35 K (Fig. 6). Upon further increasing the magnetic field from 0.1 to 1.0 T, the maximum χT values for both **II-a** and **II-b** decreased, likely because smaller spin states were mixed to the $S = 9$ state by Zeeman effects (Fig. S4 and S8, ESI†). Owing to the significantly large magnetic susceptibility under the magnetic field, the magnetization curve of **II-a** showed a

rapid increase at the small magnetic field (0.5–1.5 T) compared with the Brillouin function with $S_T = 9$, also suggesting the presence of intermolecular ferromagnetic interactions (Fig. 5b), whereas intermolecular magnetic interactions were hardly observed in **II-b** (Fig. S9, ESI†).³⁶

To elucidate the intramolecular magnetic interactions in **II-b**, the temperature dependence of χT under 0.1 T was analyzed (see Experimental Section for details, Fig. S4, ESI†). The best fitting parameters were as follows: $J_1 = 11.49 \text{ cm}^{-1}$ and $J_2 = -2.46 \text{ cm}^{-1}$, where J_1 and J_2 represent the exchange constants for V–Mn and Mn–Mn, respectively. These results revealed the large positive value for J_1 together with the significantly larger value of $|J_1|$ than that of $|J_2|$, thereby supporting the conclusion that the large spin ground state of **II-b** was engendered by the presence of strong intramolecular ferromagnetic interactions between V^{3+} and Mn^{3+} ($S_T = 1 + 2 \times 4 = 9$, Fig. 2b). The intramolecular magnetic interactions in **II-a** under 0.1 T ($J_1 = 11.25 \text{ cm}^{-1}$, $J_2 = -3.00 \text{ cm}^{-1}$; Fig. S10, ESI†)³⁷ were very close to those for **II-b**, supporting that both **II-a** and **II-b** possessed a spin ground state of 9.³⁸

All of the above-mentioned results and considerations strongly support the existence of unusually long distance intermolecular ferromagnetic interactions. In general, intermolecular interactions are not observed in POMs because the distances between paramagnetic metal oxo clusters are long enough ($> \text{ca. } 10 \text{ \AA}$) not to make superexchange pathways by bulky POM frameworks.^{20,39} There are several magnetic molecules that have been reported to show magnetic ordering induced by only intermolecular magnetic dipole interactions despite not having intermolecular exchange pathways between clusters.^{9,11} However, such magnetic dipole interactions are observed only at extremely low temperature (typically, below 2 K). In addition, for **II-a**, the dipole energy was estimated to be $E_{\text{dip}} = 0.042 \text{ K}$,⁴⁰ at which the dipole interactions were expected to play a role.⁸ This value was much smaller than 35 K, thus indicating that the intermolecular magnetic interactions in **II-a** could not be explained by simple dipole-dipole interactions.

Although **II-a** and **II-b** possessed the same anion structures and large-spin ground states ($S_T = 9$), the field-induced intermolecular ferromagnetic interactions were observed only for **II-a**. As mentioned above, the significant difference between **II-a** and **II-b** is only the molecular orientation in crystals. In addition, intermolecular interactions were not observed in a previously reported ferrimagnetic $\{\text{FeMn}_4\}$ cluster (**III**) having a smaller spin ground state of $S_T = 11/2$ (Table S6, ESI†).²³ The anion structure and crystal packing in **III** are intrinsically the same as those in **II-a**. On the basis of these results, we can deduce that the alignment of molecular orientation in the crystal and the large-spin ground state are crucial factors for the field-induced long distance intermolecular ferromagnetic interactions in **II-a**. One possible explanation is based on the magnetic field effects in chemical reactions, i.e., radical-pair mechanism or radical-triplet mechanism.⁴¹⁻⁴⁸ The magnitude of the spin-state mixing should be based on the ratio of the energy difference between the diagonal matrix elements and the magnitude of the off-diagonal matrix element, and is considered for **II-a** as follows: i) Since the Zeeman splitting for the $\{\text{VMn}_4\}$ cluster with $S_T = 9$ is much larger than that for a molecule with $S = 1/2$, the energy difference between the diagonal matrix elements should be small. ii) In the case of metal complexes with $S \geq 1$, the off-diagonal matrix element is approximated to zero-field splitting derived from the anisotropy cause by the spin-orbital coupling, which should be large when the molecular orientation is aligned. This proposed mechanism is in agreement with the intermolecular ferromagnetic interactions observed only for **II-a** from the viewpoint of the large-spin ground state, the small magnetic field-induction, and the molecular orientation.

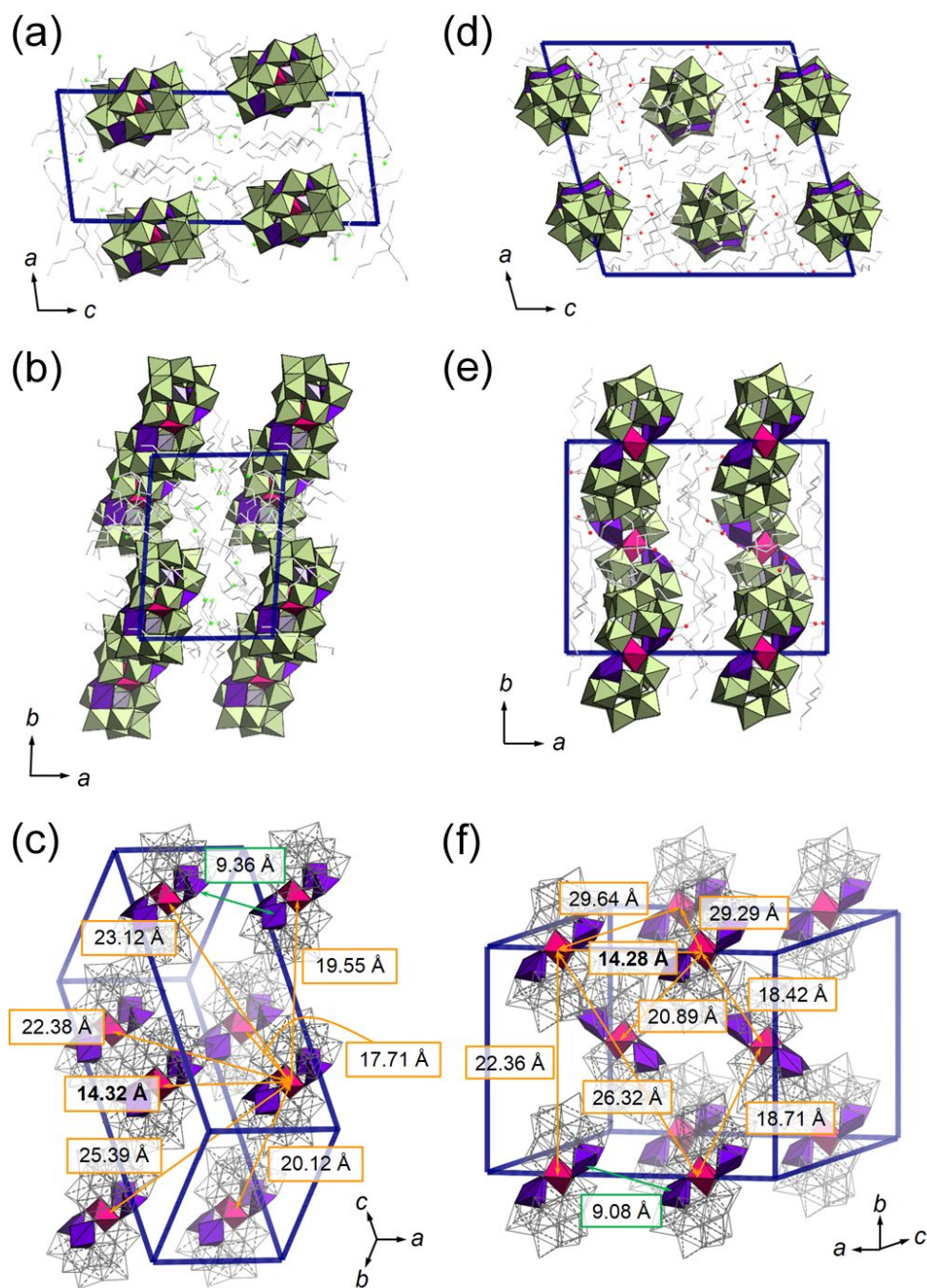


Fig. 4 Crystal structures of (a–c) **II-a** and (d–f) **II-b**. Views along the (a,d) *b*, and (b,e) *c* axis, and views displaying the distances between paramagnetic metals of (c) **II-a** and (f) **II-b**. Green, gray, pink, and purple polyhedra represent $[\text{WO}_6]^{6-}$, $[\text{SiO}_4]^{4-}$, $[\text{VO}_6]^{9-}$, and $[\text{MnO}_5]^{7-}$, respectively. Red and light green spheres represent O and Cl atoms, respectively. Gray sticks represent TBA cations. Blue grid lines represent unit cells.

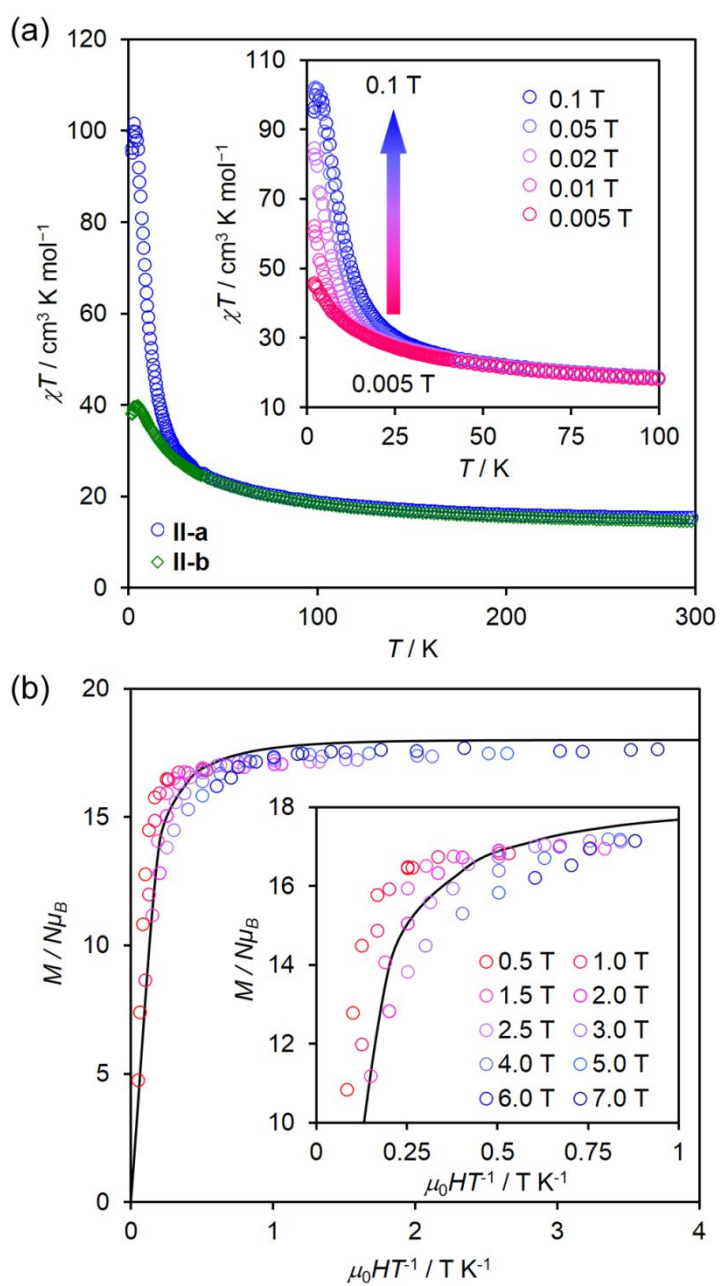


Fig. 5 (a) Temperature dependences of χT for **II-a** (blue circle) and **II-b** (green square) under 0.1 T. Inset: Temperature dependences of χT for **II-a** under various magnetic fields. (b) Low-temperature magnetization data for **II-a**. The solid line represents the curve of the Brillouin function estimated with $S_T = 9$. Inset: An enlarged view.

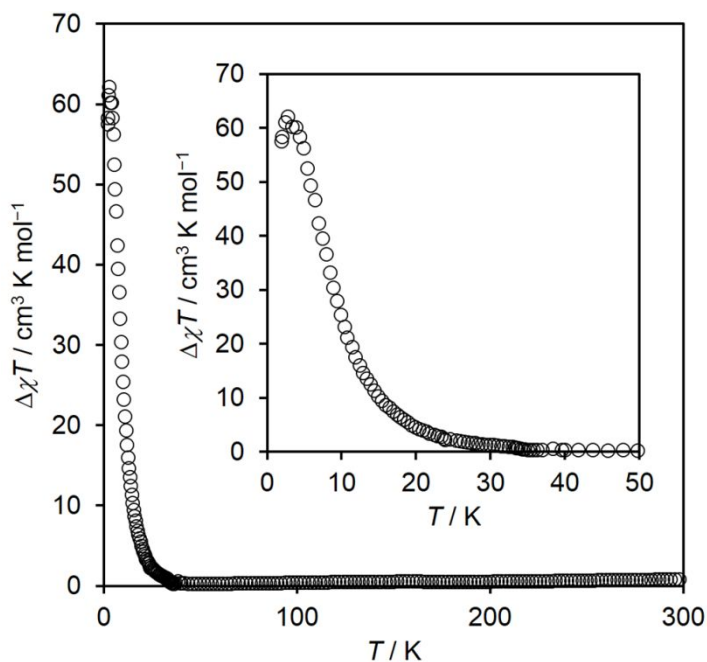


Fig. 6 Temperature dependence of $\Delta\chi T$ ($\Delta\chi T = \chi T(\text{II-a}) - \chi T(\text{II-b})$) under the applied dc field of 0.1 T. Inset: Enlarged view of temperature dependences of $\Delta\chi T$.

Conclusions

In conclusion, the orientationally aligned (**II-a**) and not aligned (**II-b**) anisotropic large spin ($S_T = 9$) molecules $\{\text{V}^{3+}\text{Mn}^{3+}_4\}$ within anisotropic trivacant lacunary POMs were synthesized by the sequential synthesis method. The unique field-induced long distance intermolecular magnetic interaction ($> 10 \text{ \AA}$) was observed in **II-a** below 35 K, presumably because of the alignment of molecular orientation and the large-spin ground state.

Experimental section

Materials

Acetone (Kanto Chemical), acetonitrile (Kanto Chemical), 1,2-dichloroethane (Kanto Chemical), nitromethane (TCI), diethyl ether (Kanto Chemical), tetra-*n*-butylammonium perchlorate (nacalai

tesque), $V(\text{acac})_3$ (Aldrich), and $Mn(\text{acac})_3$ (Aldrich) were used as received. $TBA_4H_6[A-\alpha-SiW_9O_{34}] \cdot 2H_2O$ was synthesized according to the reported procedure.²⁶

Instruments

IR spectra were measured on JASCO FT/IR-4100 using KBr disks. UV/Vis spectra were measured on JASCO V-570DS. Cold-spray ionization (CSI) mass spectra were recorded on JEOL JMS-T100CS. Thermogravimetric and differential thermal analyses (TG-DTA) were performed on Rigaku Thermo plus TG 8120. ICP-AES analyses for V, Mn, Si, and W were performed with Shimadzu ICPS-8100. Elemental analyses were performed on Elementar vario MICRO cube (for C, H, and N) at the Elemental Analysis Center of School of Science of the University of Tokyo.

X-ray Crystallography

Diffraction measurements were made on a Rigaku MicroMax-007 Saturn 724 CCD detector with graphic monochromated Mo K radiation ($\lambda = 0.71069 \text{ \AA}$, 50 kV, 24 mA) at 123 K. The data were collected and processed using CrystalClear^{49,50} and HKL2000.⁵¹ Neutral scattering factors were obtained from the standard source. In the reduction of data, Lorentz and polarization corrections were made. The structural analyses were performed using CrystalStructure⁵² and WinGX.⁵³ All structures were solved by SHELXS-97 (direct methods) and refined by SHELXL-2014.^{54,55} The metal atoms (V, Mn, Si, and W) and oxygen atoms in the POM frameworks were refined anisotropically. In the crystallographic analysis of compound **I**, large electron densities remained near the atoms at the vacant sites of lacunary POM frameworks. This is likely due to the disorder of these atoms. CCDC-1818066 (**I**), -1818067 (**II-a**), and -1818068 (**II-b**) contain the supplementary crystallographic data for this paper. The data can be obtained free of charge via www.ccdc.cam.ac.uk/conts/retrieving.html (or from the Cambridge Crystallographic Data Centre, 12, Union Road, Cambridge CB2 1EZ, UK; Fax: (+44) 1223-336-033; or deposit@ccdc.cam.ac.uk).

Bond Valence Sum (BVS) Calculations

The BVS values were calculated by the expression for the variation of the length r_{ij} of a bond between two atoms i and j in observed crystal with valence V_i .

$$V_i = \sum_j \exp\left(\frac{r'_0 - r_{ij}}{B}\right)$$

where B is constant equal to 0.37 Å, r'_0 is bond valence parameter for a given atom pair.^{56,57}

XPS Analysis

XPS analyses were performed using JEOL JPS-9000 under Mg K α radiation ($h\nu = 1253.6$ eV, 8 kV, 10 mA). The peak positions were calibrated by the O1s (530.0 eV) of oxygen atoms in POMs, and the baselines were subtracted by the Shirley method.

Electrochemistry

Cyclic voltammetric measurements were carried out with Solartron SI 1287 Electrochemical Interface. A standard three-electrode arrangement was employed with a BAS glassy carbon disk electrode as the working electrode, a platinum wire as the counter electrode, and a silver wire electrode as the pseudoreference electrode. The voltage scan rate was set at 100 mV s⁻¹, and TBAClO₄ was used as an electrolyte. The potentials were measured using Ag/AgNO₃ reference electrode (10 mM AgNO₃, 100 mM TBAClO₄ in acetonitrile, 0.55 V vs the normal hydrogen electrode (NHE)) and were converted to NHE.

Magnetic Susceptibilities

Magnetic susceptibilities of polycrystalline samples were measured on Quantum Design MPMS-XL7. Direct current (dc) field-cooling magnetic susceptibility measurements were carried out between 1.9 and 300 K under 0.005–1.0 T magnetic field. Diamagnetic corrections were applied by the diamagnetisms of the sample holder and TBA₄H₆[A- α -SiW₉O₃₄] \cdot 2H₂O. Alternating current (ac) magnetic susceptibility measurements were carried out under the zero or 0.1 T dc field and the 3.96

$\times 10^{-4}$ T ac oscillating field. Spin Hamiltonian can be expressed by the following equation: $\mathbf{H} = \mathbf{H}_{\text{SO}} + \mathbf{H}_{\text{EX}} + \mathbf{H}_{\text{CF}} + \mathbf{H}_{\text{ZEE}}$ (\mathbf{H}_{SO} , spin orbit coupling; \mathbf{H}_{EX} , exchange coupling; \mathbf{H}_{CF} , crystal field interaction; \mathbf{H}_{ZEE} , Zeeman effect). The magnetic interactions were analyzed by fitting the temperature-dependence of magnetic susceptibilities with the following isotropic spin Heisenberg–Dirac–van Vleck Hamiltonian

$$\mathbf{H}_{\text{EX}} = -2J_1(S_V \cdot S_{\text{Mn}1} + S_V \cdot S_{\text{Mn}2} + S_V \cdot S_{\text{Mn}3} + S_V \cdot S_{\text{Mn}4}) - 2J_2(S_{\text{Mn}1} \cdot S_{\text{Mn}2} + S_{\text{Mn}3} \cdot S_{\text{Mn}4})$$

where J_1 and J_2 represent exchange constants of V^{3+} – Mn^{3+} and Mn^{3+} – Mn^{3+} , respectively. The analyses were carried out by using the PHI program.⁵⁸ The g values for V^{3+} and Mn^{3+} were fixed to 2. Intermolecular magnetic interactions between $\{\text{VMn}_4\}$ clusters in **II-a** was modeled using the mean-field approximation.⁵⁹

Synthesis and characterization of $\text{TBA}_7\text{H}_{10}[(\text{A}-\alpha\text{-SiW}_9\text{O}_{34})_2\text{V}] \cdot 2\text{H}_2\text{O} \cdot \text{C}_2\text{H}_4\text{Cl}_2$ (**I**)

To a deaerated mixed solvent of acetone and water (17:3, v/v, 32 mL) of $\text{V}(\text{acac})_3$ (86.0 mg, 247 μmol), $\text{TBA}_4\text{H}_6[\text{A}-\alpha\text{-SiW}_9\text{O}_{34}] \cdot 2\text{H}_2\text{O}$ (1.60 g, 494 μmol) was added, and the resulting solution was stirred for 3 h at room temperature (ca. 20°C) under Ar atmosphere. Then, diethyl ether (240 mL) was added to the solution and brown precipitates formed were isolated by decantation. Brown powder isolated was washed with diethyl ether (30 mL) twice, followed by recrystallization from mixed solvent of 1,2-dichloroethane (32 mL) and diethyl ether (13 mL). The brown crystals of **I** suitable for X-ray crystallographic analysis were obtained (644 mg, 41% yield based on $\text{TBA}_4\text{H}_6[\text{A}-\alpha\text{-SiW}_9\text{O}_{34}] \cdot 2\text{H}_2\text{O}$). IR (KBr pellet): 2961, 2934, 2873, 1634, 1484, 1471, 1383, 1347, 1281, 1152, 1107, 1062, 1014, 991, 954, 908, 890, 813, 770, 681, 653, 560, 537, 516, 457, 377, 366, 359, 337, 325, 302, 291, 283, 267, 258, 256, 252 cm^{-1} ; UV/Vis (acetonitrile): λ (ϵ) 249 nm ($6.7 \times 10^{-4} \text{ M}^{-1} \text{ cm}^{-1}$); positive ion MS (ESI, 1,2-dichloroethane): m/z 3330 (calcd. 3330.2) $[\text{TBA}_9\text{H}_6\text{VSi}_2\text{W}_{18}\text{O}_{66}]^{2+}$, 6418 (calcd. 6418.0) $[\text{TBA}_8\text{H}_6\text{VSi}_2\text{W}_{18}\text{O}_{66}]^+$; elemental analysis calcd (%)

for $\text{TBA}_7\text{H}_{10}[(\text{SiW}_{19}\text{O}_{34})_2\text{V}]\cdot 2\text{H}_2\text{O}\cdot \text{C}_2\text{H}_4\text{Cl}_2$ ($\text{C}_{114}\text{H}_{270}\text{N}_7\text{O}_{70}\text{Si}_2\text{VW}_{18}$), C 21.57, H 4.29, N 1.55, Si 0.89, V 0.80, W 52.14; found, C 21.51, H 4.27, N 1.51, Si 0.89, V 0.82, W 53.09.

Synthesis and characterization of $\text{TBA}_7[(\text{A}-\alpha\text{-SiW}_9\text{O}_{34})_2\text{VMn}_4(\text{OH})_2]\cdot(\text{solvent})$ (**II**)

$\text{Mn}(\text{acac})_3$ (89.2 mg, 253 μmol) was added to a 1,2-dichloroethane solution (6 mL) of **I** (400 mg, 63 μmol), and the resulting solution was stirred for 1 h at room temperature (ca. 20°C). Then, diethyl ether (16 mL) was added and the solution was filtered off. The dark purple crystals of **II** (**II-a**) suitable for X-ray crystallographic analysis were obtained (336 mg, 82% yield based on **I**). **II-b** was synthesized by the recrystallization of **II** (52.5 mg, 8.1 μmol) in the mixed solvent of nitromethane (1.0 mL) and diethyl ether (2.9 mL). (42.3 mg). IR (KBr pellet): 2961, 2935, 2873, 1635, 1484, 1381, 1152, 1107, 1056, 1014, 987, 957, 934, 923, 892, 876, 788, 709, 643, 551, 534, 409, 387, 374, 333, 279, 258 cm^{-1} ; UV/Vis (acetonitrile): λ (ϵ) 268 nm ($5.9 \times 10^{-4} \text{ M}^{-1} \text{ cm}^{-1}$); positive ion MS (ESI, 1,2-dichloroethane): m/z 3470 (calcd. 3470.1) $[\text{TBA}_9\text{H}_2\text{VMn}_4\text{Si}_2\text{W}_{18}\text{O}_{70}]^{2+}$, 6698 (calcd. 6697.7) $[\text{TBA}_8\text{H}_2\text{VMn}_4\text{Si}_2\text{W}_{18}\text{O}_{70}]^+$; elemental analysis calcd (%) for **II-a** ($\text{TBA}_7[(\text{SiW}_9\text{O}_{34})_2\text{VMn}_4(\text{OH})_2]\cdot \text{H}_2\text{O}$, $\text{C}_{112}\text{H}_{256}\text{N}_7\text{O}_{71}\text{Si}_2\text{VMn}_4\text{W}_{18}$), C 20.78, H 4.00, N 1.52, Si 0.87, V 0.79, Mn 3.40, W 51.12; found, C 20.74, H 3.96, N 1.50, Si 0.83, V 0.78, Mn 3.30, W 51.80; elemental analysis calcd (%) for **II-b** ($\text{TBA}_7[(\text{SiW}_9\text{O}_{34})_2\text{VMn}_4(\text{OH})_2]\cdot 10\text{H}_2\text{O}\cdot \text{CH}_3\text{NO}_2$, $\text{C}_{113}\text{H}_{277}\text{N}_8\text{O}_{82}\text{Si}_2\text{VMn}_4\text{W}_{18}$), C 20.27, H 4.17, N 1.67, Si 0.84, V 0.76, Mn 3.28, W 49.41; found, C 20.69, H 4.03, N 1.56, Si 0.79, V 0.71, Mn 2.98, W 46.46.

Acknowledgements

We thank Prof. Leroy Cronin, University of Glasgow, for his thoughtful discussion and proofreading of this manuscript. We thank Mr. S. Sasaki, the University of Tokyo, for his help with elemental analysis. This work was supported in part by JSPS KAKENHI Grant Numbers 18H04500, 17H06375, 17H03037, 15J09840 and JST PRESTO Grant Number JPMJPR18T7. T. M. was supported by the JSPS through a Research Fellowship for Young Scientists.

Conflicts of interest

There are no conflicts to declare.

Notes and references

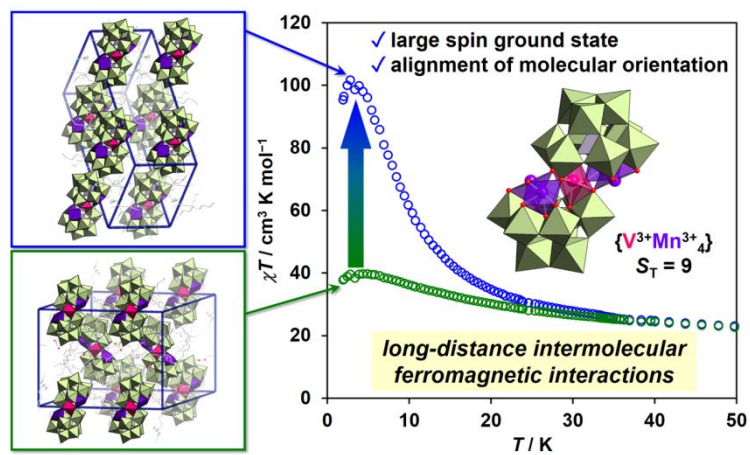
- 1 G. M. Whitesides and B. Grzybowski, *Science*, 2002, **295**, 2418.
- 2 S. C. Glotzer and M. J. Solomon, *Nat. Mater.*, 2007, **6**, 557.
- 3 K. L. Young, M. L. Personick, M. Engel, P. F. Damasceno, S. N. Barnaby, R. Bleher, T. Li, S. C. Glotzer, B. Lee and C. A. Mirkin, *Angew. Chem., Int. Ed.*, 2013, **52**, 13980.
- 4 C. J. Milios and R. E. P. Winpenny, Cluster-Based Single-Molecule Magnets. In *Molecular Nanomagnets and Related Phenomena, Structure and Bonding*, S. Gao Ed., Springer: Berlin, 2014, Vol. 164.
- 5 J. F. Fernández and J. J. Alonso, *Phys. Rev. B*, 2000, **62**, 53.
- 6 P. Panissod and M. Drillon, Magnetic Ordering due to Dipolar Interaction in Low Dimensional Materials. In *Magnetism: Molecules to Materials IV: Nanosized Magnetic Materials*, J. S. Miller and M. Drillon, Eds., Wiley-VCH, Weinheim, 2002.
- 7 W. Wernsdorfer, N. Aliaga-Alcalde, D. N. Hendrickson and G. Christou, *Nature*, 2002, **416**, 406.
- 8 M. Affronte, J. C. Lasjaunias, W. Wernsdorfer, R. Sessoli, D. Gatteschi, S. L. Heath, A. Fort and A. Rettori, *Phys. Rev. B.*, 2002, **66**, 064408.

- 9 A. Morello, F. L. Mettes, F. Luis, J. F. Fernández, J. Krzystek, G. Aromí, G. Christou and L. De Jongh, *J. Phys. Rev. Lett.*, 2003, **90**, 017206.
- 10 W. Wernsdorfer, S. Bhaduri, A. Vinslava and G. Christou, *Phys. Rev. B*, 2005, **72**, 214429.
- 11 C. Vecchini, D. H. Ryan, L. M. D. Cranswick, M. Evangelisti, W. Kockelmann, P. G. Radaelli, A. Candini, M. Affronte, I. A. Gass, E. K. Brechin and O. Moze, *Phys. Rev. B*, 2008, **77**, 224403.
- 12 M. Evangelisti, A. Candini, A. Ghirri, M. Affronte, G. W. Powell, I. A. Gass, P. A. Wood, S. Parsons, E. K. Brechin, D. Collison and S. L. Heath, *Phys. Rev. Lett.*, 2006, **97**, 167202.
- 13 J. Larionova, M. Gross, M. Pilkington, H. Andres, H. Stoeckli-Evans, H. U. Güdel and S. Decurtins, *Angew. Chem., Int. Ed.*, 2000, **39**, 1605.
- 14 W. Luo, S. R. Nagel, T. F. Rosenbaum and R. E. Rosensweig, *Phys. Rev. Lett.*, 1991, **67**, 2721.
- 15 M. Rotter, M. Loewenhaupt, M. Doerr, A. Lindbaum, H. Sassik, K. Ziebeck and B. Beuneu, *Phys. Rev. B*, 2003, **68**, 144418.
- 16 *Advances in Inorganic Chemistry*; R. Eldik and L. Cronin, Eds.; Elsevier Academic Press: Amsterdam, 2017, Vol. 69.
- 17 Y.-F. Song and R. Tsunashima, *Chem. Soc. Rev.*, 2012, **41**, 7384.
- 18 O. Oms, A. Dolbecq and P. Mialane, *Chem. Soc. Rev.*, 2012, **41**, 7497.
- 19 S.-T. Zheng and G.-Y. Yang, *Chem. Soc. Rev.*, 2012, **41**, 7623.
- 20 U. Kortz, A. Müller, J. Van Slageren, J. Schnack, N. S. Dalal and M. Dressel, *Coord. Chem. Rev.*, 2009, **253**, 2315.
- 21 K. Suzuki, N. Mizuno and K. Yamaguchi, *ACS Catal.*, 2018, **8**, 10809.
- 22 R. Sato, K. Suzuki, T. Minato, M. Shinoe, K. Yamaguchi and N. Mizuno, *Chem. Commun.*, 2015, **51**, 4081.
- 23 K. Suzuki, R. Sato, T. Minato, M. Shinoe, K. Yamaguchi and N. Mizuno, *Dalton Trans.*, 2015, **44**, 14220.
- 24 R. Sato, K. Suzuki, T. Minato, K. Yamaguchi, N. Mizuno, *Inorg. Chem.*, 2016, **55**, 2023.
- 25 T. Minato, K. Suzuki, Y. Ohata, K. Yamaguchi and N. Mizuno, *Chem. Commun.*, 2017, **53**, 753.

- 26 T. Minato, K. Suzuki, K. Kamata and N. Mizuno, *Chem. Eur. J.*, 2014, **20**, 5946.
- 27 When the reaction was carried out in air, V^{3+} was oxidized to V^{4+} and **I** could not be obtained (Fig. S11, ESI†).
- 28 G. Silversmit, D. Depla, H. Poelman, G. B. Marin and R. D. Gryse, *J. Electron. Spectrosc. Relat. Phenom.*, 2004, **135**, 167.
- 29 The sharp drop of χT value for **I** at the lowest temperature was presumably caused by the strong distortion of $[V^{3+}O_6]^{9-}$ moiety. In a temperature range of 80–300 K, an accurate diamagnetic correction was difficult due to only a small spin ($S = 1$) within large diamagnetic POM clusters $[A-\alpha-SiW_9O_{34}]^{10-}$, and thus the average χT value for separately synthesized **I** was observed with a large standard error of the mean although the average χT value of $0.90 \pm 0.096 \text{ cm}^3 \text{ K mol}^{-1}$ at 300 K still supported the valence of V^{3+} . The χT values were smaller than those in a system of $S = 1$ and $g = 2.00$ presumably because of a significant contribution of temperature independent paramagnetism and/or a slightly small g factor.
- 30 The dc magnetic susceptibility of **I** does not change, even when stored in air for 1 week, indicating that **I** is stable. The CSI mass spectrum showed that **I** is also stable in solution (Fig. S3a, ESI†).
- 31 The cyclic voltammogram of **I** in acetonitrile showed a reversible V^{3+}/V^{4+} redox couple at $E_{1/2} = 0.67 \text{ V}$ (vs. NHE) (Fig. S12, ESI†), which shifted to a positive value compared with that of $[PW_{11}VO_{40}]^{4-}$ (V^{3+}/V^{4+} , $E_{1/2} = 0.25 \text{ V}$ (vs. NHE)), indicating the stabilization of V^{3+} state. See: C. Li, R. Cao, K. P. O'Halloran, H. Ma and L. Wu, *Electrochim. Acta* 2008, **54**, 484.
- 32 The introduction of V^{3+} cations into lacunary POMs has not been reported although isopolyoxometalates containing V^{3+} have been synthesized. See for example: L. J. Batchelor, R. Shaw, S. J. Markey, M. Helliwell and E. J. L. McInnes, *Chem. Eur. J.*, 2010, **16**, 5554.
- 33 The χT values of **II-a** and **II-b** at 300 K are larger than the expected values for free ions of one V^{3+} and four Mn^{3+} ($\chi T = 13 \text{ cm}^3 \text{ K mol}^{-1}$) likely because χT values did not converge even at 300 K due to the dominant intra- and inter-molecular ferromagnetic interactions.
- 34 There has been only a few reports on the POMs possessing the larger spin ground state than compound **II**. For example, Y. Zhen, B. Liu, L. Li, D. Wang, Y. Ma, H. Hu, S. Gao and G. Xue, *Dalton Trans.*, 2013, **42**, 58.
- 35 The Brillouin function was plotted using $J = S_{\text{total}} = 9$ and $g_J = g_e = 2.00$.

- 36 J. S. Miller, *Chem. Soc. Rev.*, 2011, **40**, 3266.
- 37 The intermolecular interaction in **II-a** was analyzed by assuming intermolecular exchange interactions and fitting experimental χT values in a temperature range of 10–300 K based on the mean-field approximation, indicating the intermolecular ferromagnetic interaction ($zJ = 0.092 \text{ cm}^{-1}$).
- 38 The obtained J_2 values for **II-a** and **II-b** were similar to those for $\{\text{MMn}_4\}$ ($M = \text{Cr}^{3+}, \text{Mn}^{3+}, \text{Fe}^{3+}, \text{Co}^{2+}, \text{Ni}^{2+}, \text{Cu}^{2+}, \text{Ga}^{3+}$) clusters within **SiW9**,^{23,25} whereas J_1 values were the first examples for elucidating the superexchange interaction of $\text{V}^{3+}\text{-O-Mn}^{3+}$.
- 39 J. M. Clemente-Juan, E. Coronado and A. Gaita-Ariño, *Chem. Soc. Rev.*, 2012, **41**, 7464.
- 40 The dipole energy was calculated with the following formula: $E_{\text{dip}} = \mu_0(g\mu_B S_T)^2/4\pi V$, where V is the volume of the unit cell divided by the number of molecules per unit cell.^{5,9}
- 41 Y. Sakaguchi, H. Hayashi, H. Murai and Y. J. I'Haya, *Chem. Phys. Lett.*, 1984, **110**, 275.
- 42 C. D. Buckley, D. A. Hunter, P. J. Hore and K. A. McLauchlan, *Chem. Phys. Lett.*, 1987, **135**, 307.
- 43 K. Tominaga, S. Yamauchi and N. Hirota, *N. J. Chem. Phys.*, 1990, **92**, 5175.
- 44 C. Blättler, F. Jent and H. Paul, *Chem. Phys. Lett.*, 1990, **166**, 375.
- 45 A. Kawai, T. Okutsu, K. Obi, *J. Phys. Chem.*, 1991, **95**, 9130.
- 46 A. Kawai and K. Obi, *J. Phys. Chem.*, 1992, **96**, 52.
- 47 N. J. Turro, I. V. Khudyakov, S. H. Bossmann and D. W. Dwyer, *J. Phys. Chem.*, 1993, **97**, 1138.
- 48 K. Ishii, T. Ishizaki and N. Kobayashi, *J. Chem. Soc., Dalton Trans.*, 2001, 3227.
- 49 *CrystalClear* 1.3.6, Rigaku and Rigaku/MSC, The Woodlands, TX.
- 50 J. W. Pflugrath, *Acta Crystallogr.*, 1999, **D55**, 1718.
- 51 Z. Otwinowski and W. Minor; In *Macromolecular Crystallography, Part A*; C. W. Carter, Jr. and R. M. Sweet, Eds., Academic press: New York, **1997**; Vol. 276, p 307.
- 52 *CrystalStructure* 3.8, Rigaku and Rigaku/MSC, The Woodlands, TX.
- 53 L. J. Farrugia, *J. Appl. Crystallogr.*, 1999, **32**, 837.

- 54 G. M. Sheldrick, *SHELX97, Programs for Crystal Structure Analysis*, Release 97-2; University of Göttingen: Göttingen, Germany, 1997.
- 55 G. M. Sheldrick, *SHELX-2014, Programs for Crystal Structure Analysis*, University of Göttingen: Göttingen, Germany, 2014.
- 56 I. D. Brown, and D. Altermatt, *Acta Crystallogr.*, 1985, **B41**, 244.
- 57 N. E. Brese, M. O'Keeffe, *Acta Crystallogr.*, 1991, **B47**, 192.
- 58 N. F. Chilton, R. P. Anderson, L. D. Turner, A. Soncini and K. S. Murray, *J. Comput. Chem.*, 2013, **34**, 1164.
- 59 C. J. O'Connor, In *Progress in Inorganic Chemistry*; S. J. Lipard, Eds.; John Wiley & Sons: New York, 2007; Vol. 29, p203.



Orientationally aligned anisotropic large-spin polyoxometalate clusters exhibited unusual long-distance intermolecular ferromagnetic interactions below 35 K under a small magnetic field.